Les Houches lectures on optical lattices
30 September – 11 October 2019

Hélène Perrin
helene.perrin[at]univ-paris13.fr

Optical lattices

Contents

Introduction

Optical lattices, first developed together with laser cooling, are now a common and important tool for the manipulation of quantum gases, in particular in the frame of lattice clocks or quantum simulation. They make use of the periodic dipole potentials generated with laser sources in a standing wave configuration.

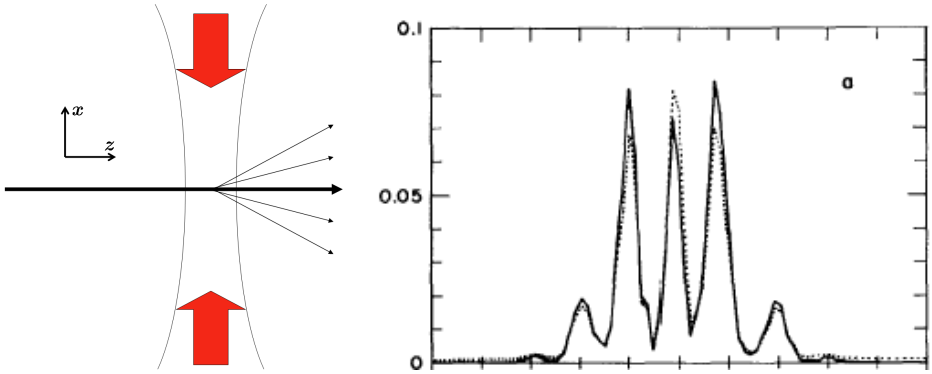

Figure 1: Diffraction of an atomic sodium beam by a stationary standing wave. Left: sketch of the experiment. Right: number of atoms detected as a function of position in the far field, revealing diffraction peaks in transverse momentum at $p_x = 0, \pm 2\hbar k, \pm 4\hbar k$. Figure from [1].

1D Depending on the laser beam configuration, we have access to various lattice geometries. The simplest situation consists in two counterpropagating plane waves $\pm\mathbf{k} = \pm k\mathbf{e}_x$ with the same frequency $\omega = ck$ and parallel polarizations, which produce a standing wave giving rise to a 1D periodic potential $V(x) = V_0 \sin^2(kx) = V_0 \left[1 - \cos(2kx)\right]/2$ of period $a = \lambda/2$ where $\lambda = 2\pi/k$. V couples momentum states along x such that $p'_x = p_x \pm 2\hbar k$.

One of first application of one-dimensional standing waves is atomic diffraction. The phenomenon is equivalent to light diffraction on a grating.

Diffraction by a standing wave can be observed in two main opposite regimes. In the thin grating limit, when the interaction time of the atoms with light is shorter than the inverse of the recoil frequency $\omega_{\rm rec} = \hbar k^2/(2M)$, the recoil energy $E_{\rm rec} = \hbar\omega_{\rm rec}$ is not resolved by the wide Fourier width of the pulse[1], and an atom can be diffracted into several diffraction peaks, with a distribution weighted by the square of Bessel functions. The new atom momentum differs from the incoming momentum by $n2\hbar k\mathbf{e}_x$ in the direction x of the standing wave, corresponding to redistribution of n photons from one laser beam to the other. Diffraction of a sodium beam by a laser standing wave has been demonstrated in the 80's [1], see Fig. 1.

On the other hand, in the thick grating regime i.e. for interaction times with the light larger than $\omega_{\rm rec}^{-1}$, the recoil energy is resolved. Diffraction can occur only for certain angles of the incoming velocity, in order to conserve both momentum and energy: $\mathbf{p}_\perp - \hbar k\mathbf{e}_x$ is coupled to $\mathbf{p}_\perp + \hbar k\mathbf{e}_x$ where $\mathbf{p}_\perp$ is the atomic momentum in the direction orthogonal to the standing wave. This regime corresponds to Bragg diffraction, and is widely used in atom interferometry for inertial sensing, as the two states $|\mathbf{p}_\perp \pm \hbar k\mathbf{e}_x\rangle$ are coupled by the standing wave in an isolated 2-level system, which allows controlled Rabi oscillations between these states. A typical atom interferometer will then consist in a $\pi/2$—π—$\pi/2$ sequence using these two states. A gravimeter or a gyrometer can be realized in this way.

Beyond 1D A 3D optical lattice is obtained by superimposing at least four plane waves in different directions. Initially, 3D optical lattices were loaded from magneto-optical traps

[1]The term 'pulse' should be replaced by 'interaction time' in the case of an atomic beam crossing a time-independent standing wave. See the exercise sheet.

(MOTs) and characterized by (i) a frequency close to resonance (a few linewidths Γ), (ii) a low filling fraction (1 atom every 10–100 sites), and (iii) a significant photon scattering rate. This topic was pioneered by the group of Gilbert Grynberg at ENS [2].

Optical lattices in the context of quantum gases use far off resonant detuned light in order to suppress spontaneous emission. A 3D square lattice is obtained by superimposing three pairs of beams in all three directions, with frequencies slightly different to avoid interferences between pairs of beams. Playing with laser frequencies and polarizations, it is also possible to realize a 2D triangular lattice with three plane waves at 120° locked in phase, or a 2D 'brickwall' lattice which has the same topology than the hexagonal lattice of graphene. Starting from a degenerate quantum gas, which density is much higher than the one of a MOT, we can reach a filling of 1, 2, 3 atoms per lattice site. The seminal experiment of Greiner et al. on the observation of the Mott transition [3] opened the way to the development of quantum simulators [4].

In a lower density regime, strong optical lattices are used to reach a very tight confinement of neutral atoms, trapped in the Lamb-Dicke regime where their zero-point motion is smaller than the wavelength. This configuration is used in metrology for building optical clocks, free from Doppler effect [5].

This course will give the basics of optical lattices in the far detuned regime where spontaneous emission is very low. Useful references include

1. The 2005 review by Immanuel Bloch [6] and Markus Greiner's PhD thesis [7]
2. Lecture notes by Fabrice Gerbier http://www.lkb.upmc.fr/boseeinsteincondensates/wp-content/uploads/sites/10/2018/03/OL2018.pdf
3. Lectures at Collège de France by Jean Dalibard (in French) [8]
4. On dipole forces: the review paper by Grimm, Weidemüller and Ovchinnikov [9]

1 Band structure in a periodic potential

1.1 Bloch theorem

The Bloch theorem is fundamental for the study of a quantum particle in a periodic potential. It states that the wavefunction of the particle is necessarily of the form

$$\boxed{\psi_{\mathbf{q}}(\mathbf{r}) = u_{\mathbf{q}}(\mathbf{r}) e^{i\mathbf{q}\cdot\mathbf{r}}}$$

where $u_{\mathbf{q}}$ is periodic over the lattice (in real space) and $\mathbf{q}$ belongs to the reciprocal lattice.

In the following we will prove this theorem.

1.1.1 Translation operators

Consider a potential V, periodic in a 3D space. There exist a basis of three vectors $(\mathbf{a}_1, \mathbf{a}_2, \mathbf{a}_3)$ such that

$$V(\mathbf{r} + \mathbf{d}) = V(\mathbf{r})$$

for any $\mathbf{d}$ such that

$$\mathbf{d} = n_1\mathbf{a}_1 + n_2\mathbf{a}_2 + n_3\mathbf{a}_3 \qquad \text{with} \quad n_1, n_2, n_3 \in \mathbb{Z}.$$

The ensemble of vectors like $\mathbf{d}$

$$\mathcal{B} = \{n_1\mathbf{a}_1 + n_2\mathbf{a}_2 + n_3\mathbf{a}_3, n_1, n_2, n_3 \in \mathbb{Z}\} \tag{1}$$

is called the **Bravais lattice**. The Hamiltonian $\hat{H} = \hat{\mathbf{p}}^2/2M + V(\hat{\mathbf{r}})$ is then invariant through a translation of $\mathbf{d} \in \mathcal{B}$. As a consequence, $\hat{H}$ commutes with the three translation operators $\hat{T}_{\mathbf{a}_j}$, $j = 1, 2, 3$.

$$\hat{T}_{\mathbf{a}_j} = \exp\left(-\frac{i\mathbf{a}_j \cdot \hat{\mathbf{p}}}{\hbar}\right) \qquad \text{such that} \qquad \hat{T}_{\mathbf{a}_j}\psi(\mathbf{r}) = \hat{T}_{\mathbf{a}_j}\psi(\mathbf{r} - \mathbf{a}_j).$$

We note immediately that any two translation operators commute with each other, as they are only function of $\hat{\mathbf{p}}$. As the three $\hat{T}_{\mathbf{a}_j}$ also commute woth $\hat{H}$, we can find a common basis for all four operators.

Now we remark that

$$\hat{T}_{\mathbf{d}}^{-1} = \hat{T}_{-\mathbf{d}} = \hat{T}_{\mathbf{d}}^{\dagger}$$

which means that the translation operators are unit operators, with eigenvalues of the form $e^{-i\theta}$ (of modulus unity). θ can be any real number, but of course θ and $\theta + 2\pi$ describe the same eigenvalue. We will denote $e^{-i\theta_j}$ a given eigenvalue of $\hat{T}_{\mathbf{a}_j}$.

1.1.2 Reciprocal lattice

We introduce the **reciprocal lattice** $\mathcal{B}'$ generated by the three vectors $(\mathbf{b}_1, \mathbf{b}_2, \mathbf{b}_3)$ such that

$$\mathbf{a}_i \cdot \mathbf{b}_j = 2\pi\delta_{ij}.$$

We now define the vector $\mathbf{q}$ on the reciprocal lattice as

$$\mathbf{q} = \frac{1}{2\pi}\sum_{j=1,2,3}\theta_j\mathbf{b}_j$$

using the phase θ_j of the eigenvalue of $\hat{T}_{\mathbf{a}_j}$. The scalar product of $\mathbf{q}$ with any vector of the Bravais lattice reads

$$\mathbf{a}_i \cdot \mathbf{q} = \frac{1}{2\pi}\sum_j \theta_j \mathbf{a}_i \cdot \mathbf{b}_j = \theta_i.$$

Then $\psi_{\mathbf{q}}$, eigenvector of all the $\hat{T}_{\mathbf{a}_j}$, satisfies for all j:

$$\psi_{\mathbf{q}}(\mathbf{r} - \mathbf{a}_j) = \hat{T}_{\mathbf{a}_j}\psi_{\mathbf{q}}(\mathbf{r}) = e^{-i\theta_j}\psi_{\mathbf{q}}(\mathbf{r}) = e^{-i\mathbf{a}_j\cdot\mathbf{q}}\psi_{\mathbf{q}}(\mathbf{r}).$$

Now if we define the function $u_{\mathbf{q}}(\mathbf{r}) = e^{-i\mathbf{r}\cdot\mathbf{q}}\psi_{\mathbf{q}}(\mathbf{r})$, we have for all three $\mathbf{a}_j$:

$$u_{\mathbf{q}}(\mathbf{r} - \mathbf{a}_j) = e^{-i\mathbf{r}\cdot\mathbf{q}}e^{i\mathbf{a}_j\cdot\mathbf{q}}\psi_{\mathbf{q}}(\mathbf{r} - \mathbf{a}_j) = e^{-i\mathbf{r}\cdot\mathbf{q}}\psi_{\mathbf{q}}(\mathbf{r}) = u_{\mathbf{q}}(\mathbf{r}).$$

$u_{\mathbf{q}}$ is thus periodic over the original Bravais lattice (in real space).

We have thus proven that the eigenfunctions of $\hat{H}$ are of the form

$$\boxed{\psi_{\mathbf{q}}(\mathbf{r}) = u_{\mathbf{q}}(\mathbf{r})e^{i\mathbf{q}\cdot\mathbf{r}}} \tag{2}$$

where $u_{\mathbf{q}}$ is periodic over $\mathcal{B}$. $\mathbf{q}$ is called the **quasi-momentum**.

As the phases θ_j are defined modulo 2π, $\mathbf{q}$ is defined modulo $\mathbf{b} \in \mathcal{B}'$. We will consider to simplify that $\psi_{\mathbf{q}+\mathbf{b}}(\mathbf{r}) = \psi_{\mathbf{q}}(\mathbf{r})$ (no phase factor).

The $\psi_{\mathbf{q}}$ are called the **Bloch functions**. They constitute a basis of the Hilbert space:

$$\int \psi^*_{n,\mathbf{q}}(\mathbf{r})\psi_{n',\mathbf{q}'}(\mathbf{r})d\mathbf{r} = \delta_{nn'}\delta_{\mathbf{q},\mathbf{q}'}. \tag{3}$$

We introduced the band index n that we will discuss in Section 1.2 as well as a quantization volume L^3 and periodic boundary conditions for the normalization of $\psi_{n,\mathbf{q}}$ such that $\mathbf{q} = 2\pi/L \sum_i n_i \mathbf{e}_i$.

1.1.3 Symmetry of the energy spectrum

In the absence of a magnetic field, the Hamiltonian, quadratic in $\mathbf{p}$, is symmetric under the time reversing symmetry $\psi \to \psi^*$, $\mathbf{p} \to -\mathbf{p}$, $\mathbf{r} \to \mathbf{r}$. If $\psi_{\mathbf{q}}(\mathbf{r})$ is a solution with energy $E(\mathbf{q})$, $\psi^*_{\mathbf{q}}(\mathbf{r}) = e^{-i\mathbf{q}\cdot\mathbf{r}}u^*_{\mathbf{q}}(\mathbf{r})$ is a solution with the same energy. But as $u^*_{\mathbf{q}}(\mathbf{r})$ is a periodic function on $\mathcal{B}$, $e^{-i\mathbf{q}\cdot\mathbf{r}}u^*_{\mathbf{q}}(\mathbf{r})$ is an eigenfunction for the quasi-momentum $-\mathbf{q}$, with energy $E(-\mathbf{q})$. We conclude that the spectrum is symmetric with respect to $\mathbf{q}$:

$$\boxed{E(-\mathbf{q}) = E(\mathbf{q}).} \tag{4}$$

1.2 Energy bands

Here we will discuss the 1D case in order to simplify the notations.

$$V(x+a) = V(x) \qquad \psi_q(x) = e^{iqx}u_q(x).$$

u_q is periodic of period a, which means than we can write it with a Fourier sum:

$$u_q(x) = \sum_{j\in\mathbb{Z}} \alpha_j(q)e^{ij\frac{2\pi}{a}x}.$$

In turn, $\psi_q(x =$ writes

$$\psi_q(x) = \sum_{j\in\mathbb{Z}} \alpha_j(q)e^{i\left(q+j\frac{2\pi}{a}\right)x}.$$

ψ_q thus appears to be a series of plane waves with momenta $\hbar\left(q + j\frac{2\pi}{a}\right)$, $j \in \mathbb{Z}$, or a **comb of momenta**.

Injecting the Bloch theorem in the Hamiltonian, we get an Hamiltonian equation for u_q:

$$\left[\frac{\hat{p}^2}{2M} + V(\hat{x})\right] e^{iqx}u_x(x) = E_n(q)e^{iqx}u_q(x)$$

Using

$$\hat{p}\left(e^{iqx}u_q\right) = \hat{p}\left(e^{iqx}\right)u_q + e^{iqx}\hat{p}u_q = e^{iqx}\left(\hbar q + \hat{p}\right)u_q$$

we derive an Hamiltonian equation for u_q:

$$\boxed{\left[\frac{(\hat{p}+\hbar q)^2}{2M} + V(\hat{x})\right] u_{n,q} = E_n(q)u_{n,q}.} \tag{5}$$

For each q, there is a spectrum of eigenenergies $E_n(q)$ with eigenfunctions $u_{n,q}$. The corresponding eigenfunctions of the Hamiltonian $\hat{H}$ are $\psi_{n,q}(x) = e^{iqx}u_{n,q}(x)$ with energy $E_n(q)$. They form an orthonormal basis.

As q is defined modulo $2\pi/a$, we restrict the description to the **first Brillouin zone** (FBZ), which contains $N_s = L/a$ discretized values of q:

$$\text{First Brillouin zone:} \qquad q \in \left[-\frac{\pi}{a}, \frac{\pi}{a}\right). \tag{6}$$

The energy interval spanned by $E_n(q)$ for $q \in$ FBZ is called the n^{th} **energy band**.

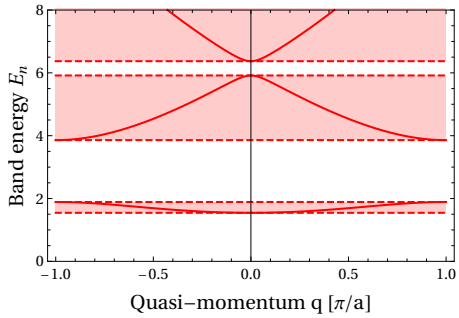

Figure 2: First energy bands in the first Brillouin zone.

1.3 Energy bands for a sinusoidal potential

We consider now specifically the case

$$V(x) = V_0 \sin^2(kx) = \frac{V_0}{2}\left[1 - \cos(2kx)\right] = \frac{V_0}{2} - \frac{V_0}{4}e^{i2kx} - \frac{V_0}{4}e^{-i2kx} \tag{7}$$

corresponding to the standing wave obtained with lasers at frequency ω and wave number k. The characteristic scales are

$$\text{lattice period:} \qquad a = \frac{\lambda}{2} = \frac{\pi}{k} \tag{8}$$

$$\text{first Brillouin zone:} \qquad q \in [-k, k) \tag{9}$$

$$\text{energy scale:} \qquad E_{\text{rec}} = \frac{\hbar^2 k^2}{2M} \tag{10}$$

$$\text{frequency scale:} \qquad \omega_{\text{rec}} = \frac{\hbar k^2}{2M}. \tag{11}$$

We will discuss the band structure in svereal limits.

1.3.1 Trivial case: $V_0 = 0$

In the absence of external potentials, the solutions are well known and are plane waves $\langle x|p\rangle \propto e^{ipx/\hbar}$. We introduce the integer j equal to the integer part of $(p + \hbar k)/(2\hbar k)$, and get

$$p = j2\hbar k + \hbar q \qquad \text{with} \quad j \in \mathbb{Z} \quad \text{and} \quad q \in [-k, k)$$

such that we can write the plane wave under the Bloch form:

$$e^{ipx/\hbar} = e^{iqx}\, e^{ij2kx}.$$

The energy reads

$$E_n(q) = \frac{p^2}{2M} = \frac{\hbar^2}{2M}(q + j2k)^2 .$$

In the band n, $j = \pm n$. Ignoring wavefunction normalization, we get

$$\begin{aligned}
n = 0 \qquad & E_0(q) = \frac{\hbar^2 q^2}{2M} = \frac{q^2}{k^2} E_{\text{rec}} \qquad & u_{0,q}(x) = 1 \\
n = 1 \qquad & E_1(q) = \frac{\hbar^2}{2M}(q \pm 2k)^2 \qquad & u_{1,q}(x) = e^{\pm 2ikx} \\
n = 2 \qquad & E_2(q) = \frac{\hbar^2}{2M}(q \pm 4k)^2 \qquad & u_{2,q}(x) = e^{\pm 4ikx}
\end{aligned}$$

The spectrum is the usual parabola folded inside the first Brillouin zone, with crossing at the edges or in the center of the Brillouin zone.

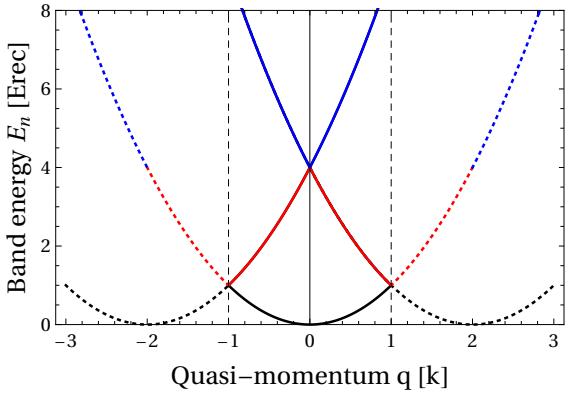

Figure 3: Energy bands for a vanishing potential. The parabola of free particles is folded inside the first Brillouin zone.

1.3.2 Band structure for $V_0 > 0$

A nonzero V_0 introduces a coupling at the crossing points. The solution can be found by numerical diagonalization in the Fourier space. We first decompose ψ_q on plane waves:

$$\psi_q(x) = \sum_j \alpha_j(q) e^{i\left(q + j\frac{2\pi}{a}\right)x} = \sum_j \alpha_j(q) e^{i(q+j2k)x} \tag{12}$$

then inject this expression in the Hamiltonian equation:

$$E_n(q)\psi_q = \hat{H}\psi_q = \left[\frac{\hat{p}^2}{2M} + V_0(\hat{x})\right]\psi_q$$

$$\begin{aligned}
E_n(q)\sum_j \alpha_j(q) e^{i(q+j2k)x} = & \sum_j \frac{\hbar^2}{2M}(q + j2k)^2 \alpha_j(q) e^{i(q+j2k)x} \\
& + \left(\frac{V_0}{2} - \frac{V_0}{4}e^{i2kx} - \frac{V_0}{4}e^{-i2kx}\right)\sum_j \alpha_j(q) e^{i(q+j2k)x}
\end{aligned}$$

which finally gives a series of coupled equations for the coefficients $\alpha_j(q)$

$$\left[\frac{\hbar^2}{2M}(q + 2jk)^2 + \frac{V_0}{2} - E_n(q)\right]\alpha_j(q) - \frac{V_0}{4}\alpha_{j-1}(q) - \frac{V_0}{4}\alpha_{j+1}(q) = 0$$

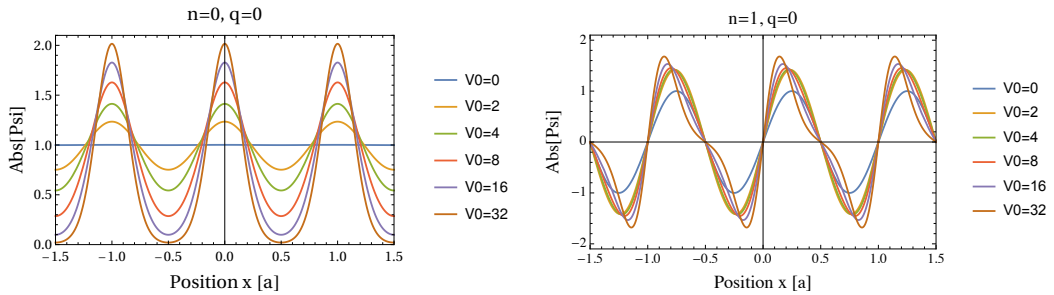

Figure 4: Modulus of the Bloch functions $|\psi_{n,q}(x)| = |u_{n,q}(x)|$ at $q = 0$ for $n = 0$ (left) and $n = 1$ (right) and for $V_0 = 0, 2, 4, 8, 16, 32 E_{\rm rec}$.

that we solve numerically. The Bloch functions for the two fisrt bands and various values of V_0 are shown on Fig. 4.

Weak lattice For V_0 small ($V_0 \lesssim E_{\rm rec}$), the solution is close to the free particle solution, with delocalized Bloch functions (see Fig. 4) and $E_n(q) \simeq \hbar^2(q \pm 2nk)^2/2M$, except where free-particle bands cross. This is the case for example for $n = 0$ and $n = 1$ close to $q = \pm k$. The dominant term in the Hamiltonian is $p^2/2M$, $V(x)$ weakly coupling p to $p \pm 2\hbar k$. Close to the edges of the Brillouin zone, this means that $|+\hbar k\rangle$ and $|-\hbar k\rangle$ are now weakly coupled, by $V_0/4$. The Hamiltonian restricted to these two states writes, at first order in V_0:

$$\hat{H} = \begin{pmatrix} E_{\rm rec} + \frac{V_0}{2} & -\frac{V_0}{4} \\ -\frac{V_0}{4} & E_{\rm rec} + \frac{V_0}{2} \end{pmatrix} = \left(E_{\rm rec} + \frac{V_0}{2}\right)\mathbb{1} - \frac{V_0}{4}\begin{pmatrix} 0 & 1 \\ 1 & 0 \end{pmatrix}.$$

The eigenstates are $(|\hbar k\rangle \pm |-\hbar k\rangle)/\sqrt{2}$, corresponding to $\psi_{0,k}(x) \propto \cos(kx)$ and $\psi_{1,k}(x) \propto \sin(kx)$, with eigenenergies

$$E = E_{\rm rec} + \frac{V_0}{2} \pm \frac{V_0}{4} \quad \Rightarrow \quad E_0(k) = E_{\rm rec} + \frac{V_0}{4}, \quad E_1(k) = E_{\rm rec} + \frac{3V_0}{4}.$$

The degeneracy at the crossing is lifted and the fundamental and the first excited bands are splitted by $V_0/2$.

N.B.: the splitting between the first and second excited band near $q = 0$ is much smaller as it involves the second order coupling of $|p = -2\hbar k\rangle$ to $|p = 2\hbar k\rangle$ through $|p = 0\rangle$. We find a splitting $V_0^2/(32E_{\rm rec})$ to lowest order in V_0.

Very deep lattice If the lattice is very deep, the confinement will provide a collection of independent traps for atoms at energies much smaller than V_0. The Bloch functions are peaked around each lattice site, see Fig. 4, and the first energy bands resemble the energy states at the bottom of an harmonic oscillator centered around each lattice well. For example, near $x = 0$, we have

$$V(x) = V_0 \sin^2(kx) \simeq V_0 k^2 x^2 = \frac{1}{2} M\omega_0^2 x^2$$

with the harmonic frequency given by

$$\omega_0 = \sqrt{2\frac{V_0 k^2}{M}} \qquad \text{or} \qquad \boxed{\hbar\omega_0 = 2\sqrt{V_0 E_{\rm rec}}.} \tag{13}$$

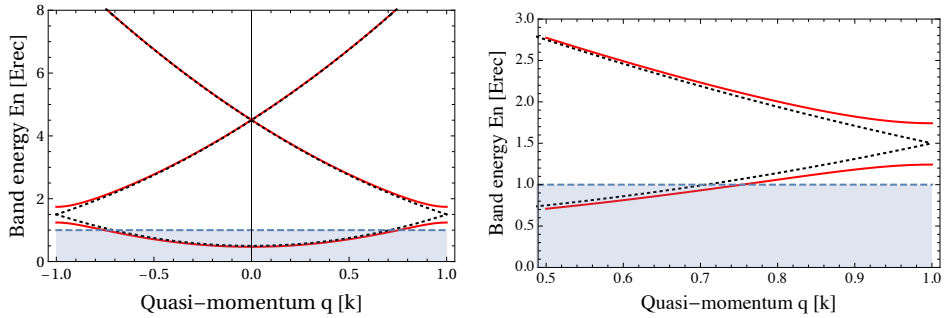

Figure 5: Left: Band structure for $V_0 = 0$ (dashed black lines) and $V_0 = E_{\rm rec}$ (full red lines). Right: If we zoom near $q = k$, we observe a gap of $\sim V_0/2$ opening between the fundamental and the first excited band. The dashed black lines are the $V_0 = 0$ solutions and the dashed blue line indicates the lattice depth V_0.

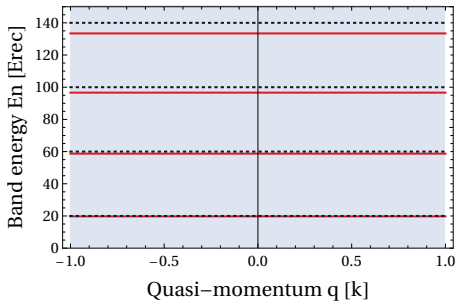

Figure 6: Red lines: first bands $n = 0$ to $n = 3$ for $V_0 = 400E_{\rm rec}$. The bands are almost flat. The dashed black lines give the harmonic levels $(n + 1/2)\hbar\omega_0$.

The energy bands are almost flat (independent of q), with $E_n(q) \simeq (n+1/2)\hbar\omega_0$. The Bloch functions are superpositions of localized functions around each site, with some dephasing. We will discuss this more in detail later with the introduction of Wannier functions.

This situation is well-suited for the realization of optical clocks. The idea is to use a narrow optical transition for the clock, between two electronic levels $|g\rangle$ and $|e\rangle$ which can also be coupled to other states by stronger dipolar transitions. If there exists a 'magic wavelength' [5] such that the electric polarizability of $|g\rangle$ and $|e\rangle$ due to these other couplings is the same, they will undergo the same light shift at this wavelength. We can then build a strong standing wave at this wavelength, with $V_0 \gg E_{\rm rec}$, to strongly confine the atoms at the bottom of the lattice wells without affecting the clock transition.

With V_0 very large, we will also have $\hbar\omega_0 \gg E_{\rm rec}$. This limit is called the Lamb-Dicke regime. Unless a strong field drives a transition from $|e, n\rangle$ to $|g, n \pm 1\rangle$ or vice versa, this transition is strongly suppressed – in particular regarding spontaneous emission – due to energy conservation: an emitted photon can only change the external energy by $E_{\rm rec}$, which is very small as compared to the difference $\hbar\omega_0$ between different vibrational states $|n\rangle$ and $|n \pm 1\rangle$. The sidebands $|g, n\rangle \to |e, n \pm 1\rangle$ are pushed away (by $\pm\omega_0$, more than the linewidth) from the carrier $|g, n\rangle \to |e, n\rangle$, which is exactly the clock frequency ω_c to be measured, see Fig. 7. This feature is at the heart of the modern strontium optical clocks.

Intermediate situation In the intermediate case (Fig. 8), the bands are well-separated but not flat. If the atomic energy is small enough, the atoms will essentially stay in the

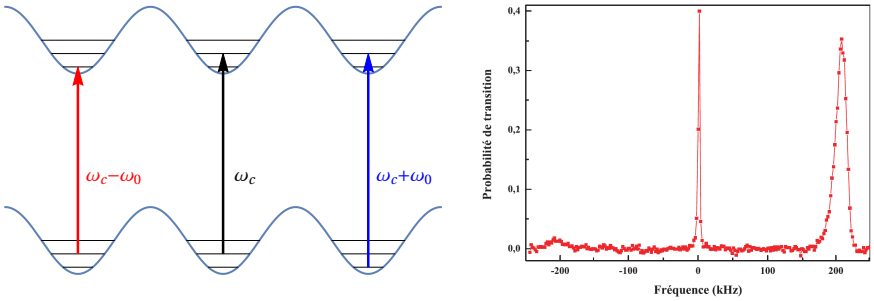

Figure 7: Left: Carrier (black, center) and sideband (red, left and blue, right) transitions in a lattice clock in the Lamb-Dicke regime. Right: Absorption spectrum of strontium 87 atoms confined in an optical lattice, with $V_0 = 940\, E_{\rm rec}$. The carrier at the clock frequency and the two sidebands at $\omega_c \pm \omega_0$ are clearly visible. The population in excited states is very small, hence the much weaker red sideband $|g, n\rangle \to |e, n-1\rangle$. Figure from [10].

fundamental band. The system is better described with either Bloch states or localized states coupled by tunneling between sites depending on the ratio $V_0/E_{\rm rec}$.

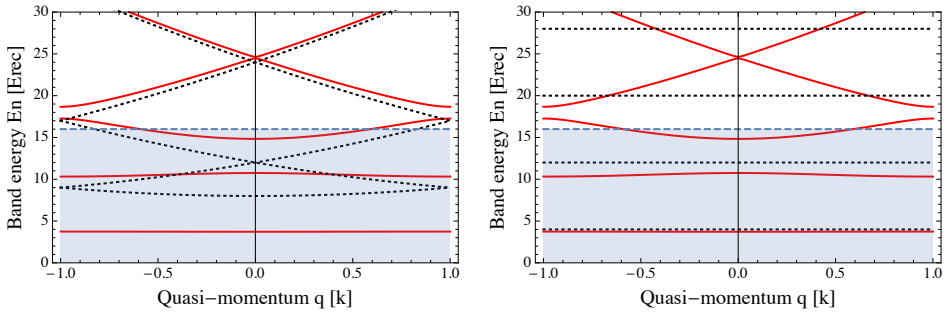

Figure 8: Band structure for $V_0 = 16\, E_{\rm rec}$, compared to the free particle case (dashed lines, left) or to the harmonic trap case (dashed lines, right). V_0 is indicated by the blue dashed line and a light blue filling. The energy bands are close to the free particle case for energies $E_n(q) > V_0$, i.e. for unbounded atoms. They are on the other hand close to the harmonic levels for deeply bound bands at low energy $E_n(q) < V_0$.

2 Dynamics in the lattice

2.1 Time-of-flight (TOF) analysis

As we have seen in the previous section, the eigenstates in the lattice are Bloch states, a sum over a comb of equally spapced momentum state. An interesting way of getting information on the momentum distribution of the atomic state in the lattice is to switch off abruptly the trapping potential. If this is done very fast, the atomic wavefunction has no time to evolve and simply remains what is was in the lattice – for example a given Bloch function. A Bloch function with a given quasi-momentum $\mathbf{q}$ is a sum over plane waves, see Eq. (12) with real momenta $\mathbf{p} = \hbar\mathbf{q} + \hbar\mathbf{Q}$ and coefficients $\alpha_{\mathbf{Q}}$, where $\mathbf{Q} \in \mathcal{B}'$

belongs to the reciprocal lattice.

$$|\psi_{\mathbf{q}}\rangle = \sum_{\mathbf{Q}\in\mathcal{B}'} \alpha_{\mathbf{Q}}(\mathbf{q})|\hbar(\mathbf{q}+\mathbf{Q})\rangle; \qquad \widetilde{\psi}_{\mathbf{q}}(\mathbf{p}, t=0) \propto \sum_{\mathbf{Q}\in\mathcal{B}'} \alpha_{\mathbf{Q}}(\mathbf{q})\,\delta(\mathbf{p}-\hbar\mathbf{q}-\hbar\mathbf{Q})$$

where $\widetilde{\psi}_{\mathbf{q}}(\mathbf{p}, t=0)$ is the Bloch wavefunction in $\mathbf{p}$ reprensentation at initial time. After a time propagation t_{TOF}, the atomic position is detected by absorption or fluorescence imaging [11]. Provided t_{TOF} is long enough, the position distribution is directly related to the initial momentum distribution through $\mathbf{r} = \mathbf{v}t_{\mathrm{TOF}} = \mathbf{p}t_{\mathrm{TOF}}/M$:

$$\begin{aligned}\psi(\mathbf{r}, t_{\mathrm{TOF}}) &\simeq \left(\frac{M}{\hbar t_{\mathrm{TOF}}}\right)^{3/2} \widetilde{\psi}_{\mathbf{q}}\left(\frac{M\mathbf{r}}{t_{\mathrm{TOF}}}, t=0\right) e^{i\frac{M\mathbf{r}^2}{2\hbar t_{\mathrm{TOF}}}} \\ &\propto \sum_{\mathbf{Q}\in\mathcal{B}'} \alpha_{\mathbf{Q}}\,\delta\left(\mathbf{r} - \frac{\hbar(\mathbf{q}+\mathbf{Q})}{M} t_{\mathrm{TOF}}\right)\end{aligned}$$

The position distribution consists in Dirac peaks weighted by $|\alpha_{\mathbf{Q}}|^2$, as expected for a Bloch state which is a comb of momenta. If $t_{\mathrm{TOF}} v_{\mathrm{rec}}$ is larger than the initial cloud size where $v_{\mathrm{rec}} = \hbar k/M$ is the recoil velocity, the peaks will be well-separated after TOF and one can observe the weights $|\alpha_{\mathbf{Q}}|^2$ over the momenta $\hbar\mathbf{q} + \hbar\mathbf{Q}$.

Figure 9 shows the momentum distribution obtained from a Bose-Einstein condensate loaded in a 3D square optical lattice, with an initial quasi-momentum $\mathbf{q} \simeq \mathbf{0}$. The atoms occupy essentially the same Bloch state, with a well-defined phase relation $e^{iqa} \simeq 1$ between lattice sites. This coherence develops into diffraction peaks after TOF. The situation is similar to the Bragg diffraction of an atomic plane wave of momentum $\mathbf{q}$ through a lattice of period a.

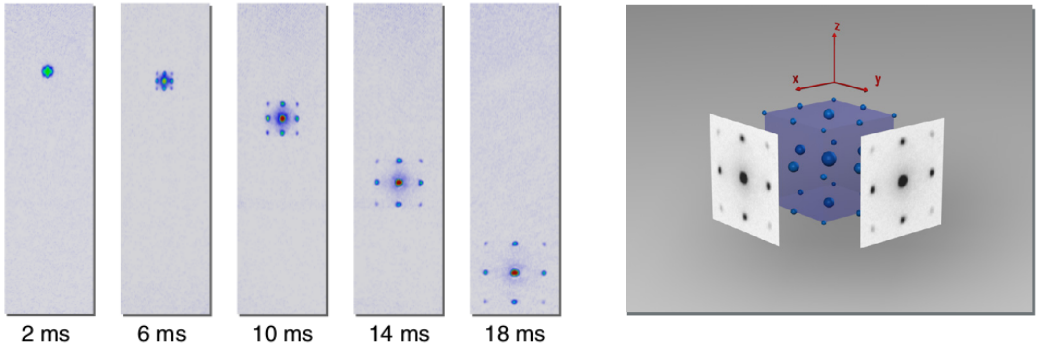

Figure 9: Left: time-of-flight expansion of a Bose-Einstein condensate loaded in a square lattice. The peaks are split by $2\hbar k$ in momentum. The coherence of the initial Bloch state translates into diffraction peaks. Right: 3D reconstruction of the pattern from two orthogonal imaging axes. Figure from [7].

2.2 Adiabatic switching

It is also interesting for a given experiment with an ensemble of atoms possibly occupying different Bloch states to be able to recover the band population. This can be done with an adiabatic opening of the lattice, i.e. a slow ramping down of the laser intensities.

Suppose we change the potential depth with time, such that the Hamiltonian is now time-dependent

$$\hat{H}(t) = \frac{\hat{\mathbf{p}}^2}{2M} + f(t)V(\hat{\mathbf{r}})$$

where $f(t)$ decribes the switching process. $\hat{H}$ still commutes with the $\hat{T}_{\mathbf{a}_j}$ operators, so does the evolution operator $\hat{U}(t)$. An initial Bloch state with quasi-momentum $\mathbf{q}$, $\psi_{\mathbf{q}}(\mathbf{r}, 0)$, which is a eigenstate of $\hat{T}_{\mathbf{a}_j}$ with eigenvalue $e^{i\mathbf{q}\cdot\mathbf{a}_j}$ at time $t = 0$, is then still an eigenstate of the $\hat{T}_{\mathbf{a}_j}$:

$$\hat{T}_{\mathbf{a}_j}\psi(\mathbf{r}, t) = \hat{T}_{\mathbf{a}_j}\hat{U}(t)\psi(\mathbf{r}, 0) = \hat{U}(t)\hat{T}_{\mathbf{a}_j}\psi(\mathbf{r}, 0) = e^{i\mathbf{q}\cdot\mathbf{a}_j}\hat{U}(t)\psi(\mathbf{r}, 0) = e^{i\mathbf{q}\cdot\mathbf{a}_j}\psi(\mathbf{r}, t).$$

$\psi(\mathbf{r}, t)$ is thus still an eigenstate with the same eigenvalue, which means that it is a Bloch state for the new potential $f(t)V(\mathbf{r})$ with the same quasi-momentum $\mathbf{q}$. **The quasi-momentum is conserved while switching the lattice.**

If, in addition, the variations of f are slow enough, such that the adiabaticity criterion is fulfilled, the weights over the various bands will also be conserved. This is true if

$$\left|\langle\psi_{n',\mathbf{q}}|\frac{d}{dt}|\psi_{n,\mathbf{q}}\rangle\right| = \left|\langle u_{n',\mathbf{q}}|\frac{d}{dt}|u_{n,\mathbf{q}}\rangle\right| \ll \frac{E_{n'}(\mathbf{q}) - E_n(\mathbf{q})}{\hbar} \qquad \text{for} \quad n \neq n'.$$

For example, starting with $p = 0$ and $f(0) = 0$, the final state will be $q = 0$ in the fundamental band $n = 0$ provided that

$$\dot{f} \ll 32\sqrt{2}\frac{E_{\text{rec}}^2}{\hbar V_0}$$

in the limit $V_0 \lesssim E_{\text{rec}}$ [8]. As the recoil frequency is on the order of a few kHz, a switching time no the order of a millisecond leads to an adiabatic switching.

An adiabatic opening of the lattice will then adiabatically connect a state $\psi_{n,\mathbf{q}}$ of the n^{th} band to the plane wave with real momentum $\hbar q \pm 2n\hbar k$. By taking a picture of the atoms after a time-of-flight, the momentum distribution translates into a position distribution allowing to identify the population in the various bands before the adiabatic switching, see Fig. 10.

2.3 Wavepacket evolution in a band

We will now consider (in one dimension) a superposition of Bloch states inside a given band, with some weight $f(q)$ over the different q, and wonder how it will evolve. We can see this superposition as a **wavepacket** in q, with a center q_0 and a width $\Delta q \ll 2k$ such that it is well localized in the FBZ. At time $t = 0$, we write

$$\psi(x, 0) = \int f(q)\psi_{n,q}(x)\,\mathrm{d}q$$

As $\Delta q \ll 2k$, we can expand the energy $E_n(q)$ around q_0:

$$E_n(q) \simeq E_n(q_0) + (q - q_0)\left.\frac{\mathrm{d}E_n}{\mathrm{d}q}\right|_{q=q_0}.$$

We define the following velocity:

$$v_{g,n} = \frac{1}{\hbar}\left.\frac{\mathrm{d}E_n}{\mathrm{d}q}\right|_{q=q_0}. \tag{14}$$

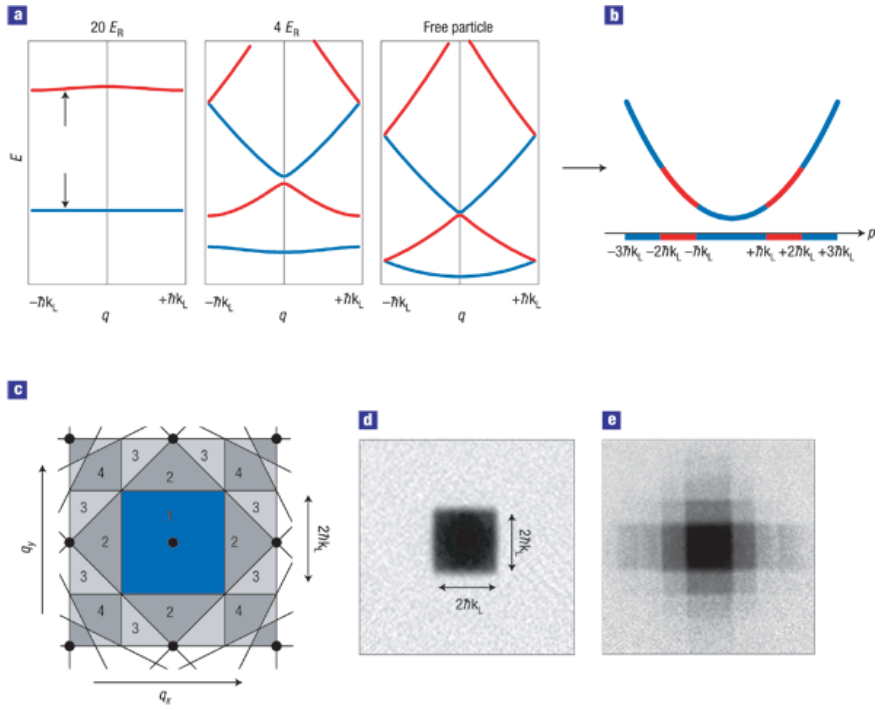

Figure 10: Adiabatic band mapping procedure. Figure from [6].

It can be interpreted as the group velocity of the wavepacket in the band n. The wavefunction at time t is

$$\psi(x,t) = \int f(q)\psi_{n,q}(x)e^{-i\frac{E_n(q)t}{\hbar}}\,\mathrm{d}q \simeq e^{-i\frac{E_n(q_0)t}{\hbar}}e^{iq_0v_{g,n}t}\int f(q)\psi_{n,q}(x)e^{-iqv_{g,n}t}\,\mathrm{d}q.$$

Setting $\omega_0 = E_n(q_0)/\hbar - q_0v_{g,n}$, using the periodicity of $u_{n,q}$ with a we remark that at time $t = a/v_{g,n}$,

$$\psi(x, t = a/v_{g,n}) = e^{-i\omega_0 t}\int f(q)u_{n,q}(x - v_{g,n}t + v_{g,n}t)e^{iq(x-v_{g,n}t)}\,\mathrm{d}q = e^{-i\omega_0 t}\psi(x - v_{g,n}t, 0).$$

Apart from a phase factor, the wavepacket after this time is the initial wavepacket translated by $v_{g,n}t$, which corresponds to a group velocity $v_{g,n}$.

At the center of the band, $v_{g,n} = 0$ and the energy can be written as

$$E_n(q) \simeq \frac{\hbar^2q^2}{2m_n^*}$$

where

$$m_n^* = \left(\frac{1}{\hbar^2}\left.\frac{\mathrm{d}^2E_n}{\mathrm{d}q^2}\right|_{q=0}\right)^{-1} \tag{15}$$

is the effective mass, which can be positive or negative. In the fundamental band $n = 0$, $m^* = m_0^* \simeq M$ for a weak lattice whereas $m^* \gg M$ for a deep lattice.

Close to $q = 0$ the group velocity thus writes

$$v_{g,n} \simeq \frac{\hbar q}{m_n^*}.$$

It is the same than for a free particle, except for a renormalization of the mass.

2.4 Bloch oscillations

We consider now the situation where, in addition to the periodic lattice, we add a constant force acting on the atom. This situation is naturally encountered in the vertical direction where gravity provides this force, $F = -Mg$. A constant initial force can also play this role when the lattice is uniformly accelerated, by using in a beam pair along an axis z two different frequencies with a linearly increasing frequency difference:

$$\omega_1 = \omega + k\alpha t \qquad \omega_2 = \omega - k\alpha t.$$

The laser phase is the integral of the frequency, and the resulting electric field is then of the form

$$E \propto e^{-i\omega t}\left(e^{-i\frac{k\alpha t^2}{2}+ikx} - ie^{i\frac{k\alpha t^2}{2}-ikx}\right)$$
$$|E|^2 \propto \sin^2\left[k\left(x - \frac{\alpha t^2}{2}\right)\right] = \sin^2\left[k\left(x - x_0(t)\right)\right].$$

The lattice is static in the frame accelerated by the constant acceleration α. In this frame, the atoms undergo a constant inertial force $F = -M\ddot{x}_0 = -M\alpha$.

The Hamiltonian can then be written as

$$\hat{H}(t) = \frac{\hat{p}^2}{2M} + V(\hat{x}) - F(t)\hat{x} = \hat{H}_0 - F(t)\hat{x}. \tag{16}$$

Let us show that the evolution of a Bloch function can be described by an equation on its quasi-momentum. We assume we start in a Bloch state with quasi-momentum q_0 such that

$$\psi(x,0) = \psi_{q_0}(x) = u_{q_0}(x)e^{iq_0x}.$$

We will first make a unitary transform to $|\tilde{\psi}\rangle = U(t)^\dagger|\psi\rangle$ with

$$U(t) = e^{-\frac{i}{\hbar}A(t)\hat{x}} \qquad \text{with} \quad A(t) = -\int_0^t F(t')\,\mathrm{d}t'.$$

Of course $\tilde{\psi}(x,0) = \psi(x,0) = u_{q_0}(x)e^{iq_0x}$. $|\tilde{\psi}\rangle$ obeys the Hamiltonian

$$\tilde{H} = i\hbar\partial_t U(t)^\dagger U(t) + U(t)^\dagger H(t) U(t).$$

Simple algebra shows that we get rid of the force $F(t)$:

$$\tilde{H}(t) = \frac{[\hat{p} - A(t)]^2}{2M} + V(\hat{x}). \tag{17}$$

$\tilde{H}$ describes a particle in a lattice with a gauge field $A(t)$. As $V(x)$ is a-periodic, $\tilde{H}(t)$ commutes with $\hat{T}_a$ at each time t, and so does the evolution operator $\tilde{U}(t_1,t_2)$ from t_1 to t_2 associated to $\tilde{H}$. We conclude that the solutions of $\tilde{H}$ are of the form (2)

$$u_q(x,t)e^{iqx}$$

where $u_q(x,t)$ is periodic with period a. The quasi-momentum q is preserved during the evolution under $\tilde{H}$. As $\tilde{\psi}(x,0)$ is a Bloch function with $q = q_0$, it will still be the case at later times:

$$\tilde{\psi}(x,t) = u_{q_0}(x,t)e^{iq_0x}.$$

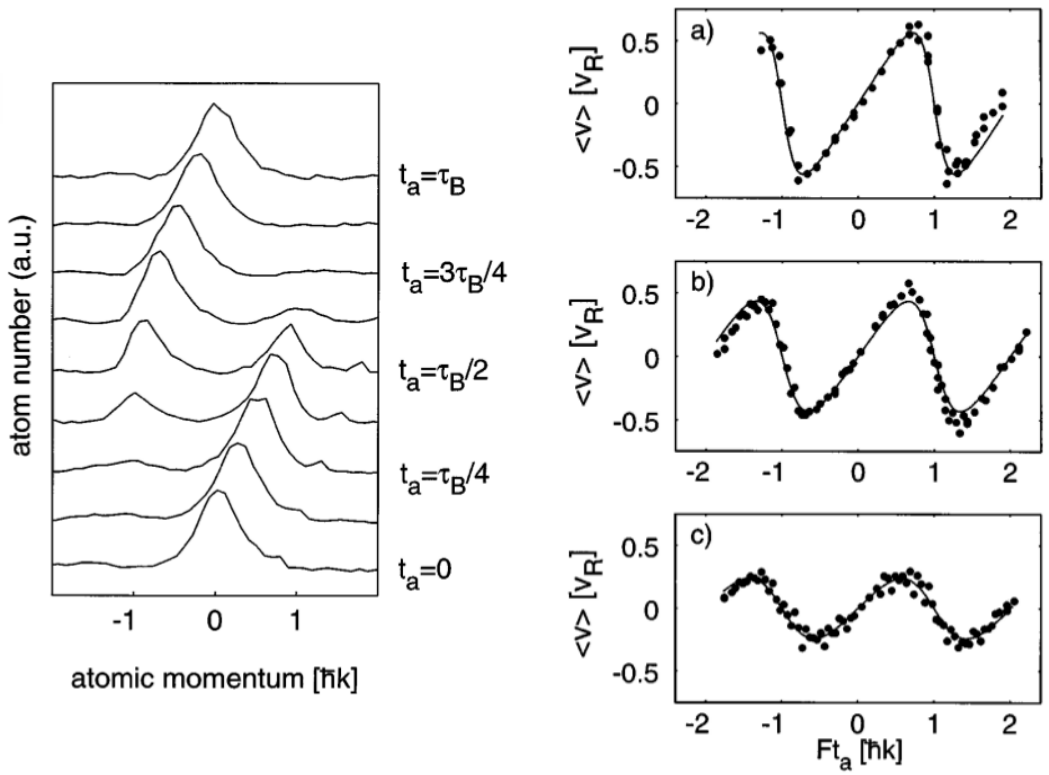

Figure 11: Bloch oscillations in an optical lattice. The momentum after a time-of-flight (left) varies periodically from $-\hbar h$ to $+\hbar k$. The group velocity (right) varies more sharply close to the edges of the FBZ when the lattice depth V_0 increases. From bottom to top: $V_0/E_{\rm rec} = 1.4, 2.3, 4.4$. Figure from [12].

Going back to $|\psi\rangle = U(t)|\tilde{\psi}\rangle$, we can write

$$\psi(x,t) = u_{q_0}(x,t)e^{iq(t)x},$$

where

$$q(t) = q_0 - \frac{1}{\hbar}A(t) = q_0 + \frac{1}{\hbar}\int_0^t F(t')\,\mathrm{d}t'. \tag{18}$$

The wave function is a Bloch function with a quasi momentum which evolves under the force $F(t)$, as a real momentum would:

$$\hbar\dot{q} = F(t). \tag{19}$$

In the case where the force F is constant, the state will come back to its initial value when $q(t)$ has increased by $2\pi/a$, see Fig. 11, i.e. after a time

$$\tau_B = \frac{h}{Fa}.$$

This is called the Bloch time. The state evolution is periodic at the Bloch frequency

$$\omega_B = \frac{Fa}{\hbar}. \tag{20}$$

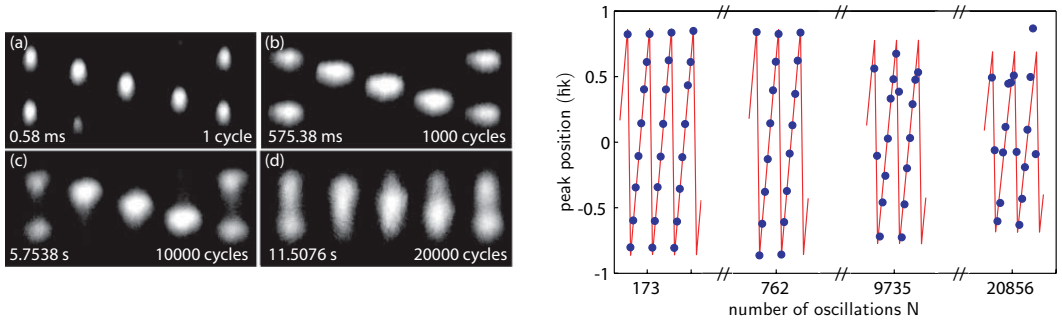

Figure 12: Up to 20,000 Bloch oscillations were observed for cesium atoms in an optical lattice, using a very cold sample (a BEC) with no interactions, cancelled with a Feshbach resonance. Left: quasi-momentum distribution in the FBZ observed after a time-of-flight. Right: Average quasi-momentum as a function the number of Bloch periods. Figure from [14].

$\hbar\omega_B = Fa$ is the energy difference between two consecutive lattice minima. The existence of periodic modulation of q can be used to measure either g or h/M very precisely [13] in a vertical lattice of period $\lambda/2$, where the Bloch frequency reads

$$\omega_B = \frac{Mg\lambda}{2\hbar} = \pi\frac{g\lambda}{h/M}.$$

A record number of oscillations of 20000 has been reported using a BEC where the interactions are tuned to zero with a Feshbach resonance [14], see Fig. 12.

In addition, Bloch oscillations provide a way to give a controlled momentum kick of $2n\hbar k$ to atoms [15], which can be used for building large area atom interferometers [16,17]. To this aim, a pair of lasers with different frequencies is applied such that atoms start Bloch oscillations in the frame moving with the lattice, resulting in an acceleration in the laboratory frame. After n Bloch periods, the momentum change is exactly $2n\hbar k$.

Bloch oscillations can be interpreted in terms of Bragg diffraction: when an atom reaches the edge of the Brillouin zone with a momentum $\hbar k$, it has exactly the resonant velocity for a Bragg diffraction, conserving both energy and momentum, and ends in the $-\hbar k$ state. Two photons are exchanged with the standing wave, one being absorbed in one beam while the other is emitted in a stimulated emission process in the other beam.

3 Deep lattices: from Wannier to Bose-Hubbard

We have seen that for V_0 larger than a few $E_{\rm rec}$, the lowest band is almost flat with an energy close to the energy of the harmonic oscillator at the bottom of a given well. In fact, in this case the $u_{\mathbf{q}}(\mathbf{r})$ periodic part of the wavefunction resembles a series of groundstates of the harmonic oscillator located at the lattice minima – lattice sites. In order to get a description more appropriate for this case of localized wavefunctions, we will introduce the Wannier functions, which describes the state in the point of view of the lattice sites.

3.1 Wannier functions

Consider the 1D case with a lattice potential $V(x) = V_0 \sin^2(kx)$, Bloch function $\psi_{n,q}(x)$ with energies $E_n(q)$. The minima of $V(x)$ are located at points

$$x_j = ja, \qquad j \in \mathbb{Z}.$$

We define the Wannier function for site j in band n as:

$$W_{n,j}(x) = \frac{1}{\sqrt{N_s}} \sum_{q \in \mathrm{FBZ}} \psi_{n,q}(x)\, e^{-ijqa} \tag{21}$$

where $N_s = L/a$ is the number of sites (a large number). We note immediately that

$$\begin{aligned} W_{n,j}(x) &= \frac{1}{\sqrt{N_s}} \sum_{q \in \mathrm{FBZ}} u_{n,q}(x)\, e^{iq(x-ja)} \\ &= \frac{1}{\sqrt{N_s}} \sum_{q \in \mathrm{FBZ}} u_{n,q}(x-ja)\, e^{iq(x-ja)} \\ &= \frac{1}{\sqrt{N_s}} \sum_{q \in \mathrm{FBZ}} \psi_{n,q}(x-ja) = W_{n,0}(x-ja) \end{aligned}$$

The Wannier function at site j is nothing but the Wannier function at site 0 shifted by ja. It is thus enough to study the well $x = 0$ in order to deduce all the Wn, j.

N.B. The Wannier function depends on the phase choice of the Bloch functions. The is a choice sich that $W_{n,j} \in \mathbb{R}$ and $W_{n,j}$ is either even or odd, and decays exponentially with x.

The Bloch functions can be written in terms of the Wannier functions, in the spirit of a Fourier series:

$$\begin{aligned} \frac{1}{\sqrt{N_s}} \sum_j W_{n,j}(x)\, e^{ijqa} &= \frac{1}{N_s} \sum_j e^{ijqa} \sum_{q' \in \mathrm{FBZ}} \psi_{n,q'}(x)\, e^{-ijq'a} \\ &= \frac{1}{N_s} \sum_{q' \in \mathrm{FBZ}} \psi_{n,q'}(x) \sum_j e^{ij(q-q')a} \\ &= \frac{1}{N_s} \sum_{q' \in \mathrm{FBZ}} \psi_{n,q'}(x) N_s \tilde{\delta}_{q,q'} \\ &= \psi_{n,q}(x) \end{aligned}$$

where the $\tilde{\delta}$ sign means that $q' = q$ modulo $2\pi/a$. We can thus give $\psi_{n,q}$ as a function of $W_{n,0}$:

$$\boxed{\psi_{n,q}(x) = \frac{1}{\sqrt{N_s}} \sum_j W_{n,0}(x-ja)\, e^{ijqa}.} \tag{22}$$

The Wannier functions form a basis of the function space:

$$\int W_{n,j}(x) W_{n',j'}(x)\, \mathrm{d}x = \delta_{n,n'} \delta_{j,j'}. \tag{23}$$

In particular, as this is also true for $W_{n,0}(x)$ and $W_{n,j}(x) = W_{n,0}(x-ja)$, it means than $W_{n,0}$ always has positive and negative values. This is clear on Fig. 13, which gives examples of Wannier functions for various values of V_0. We also remark that $W_{n,0}$ is more and more peaked for increasing values of V_0.

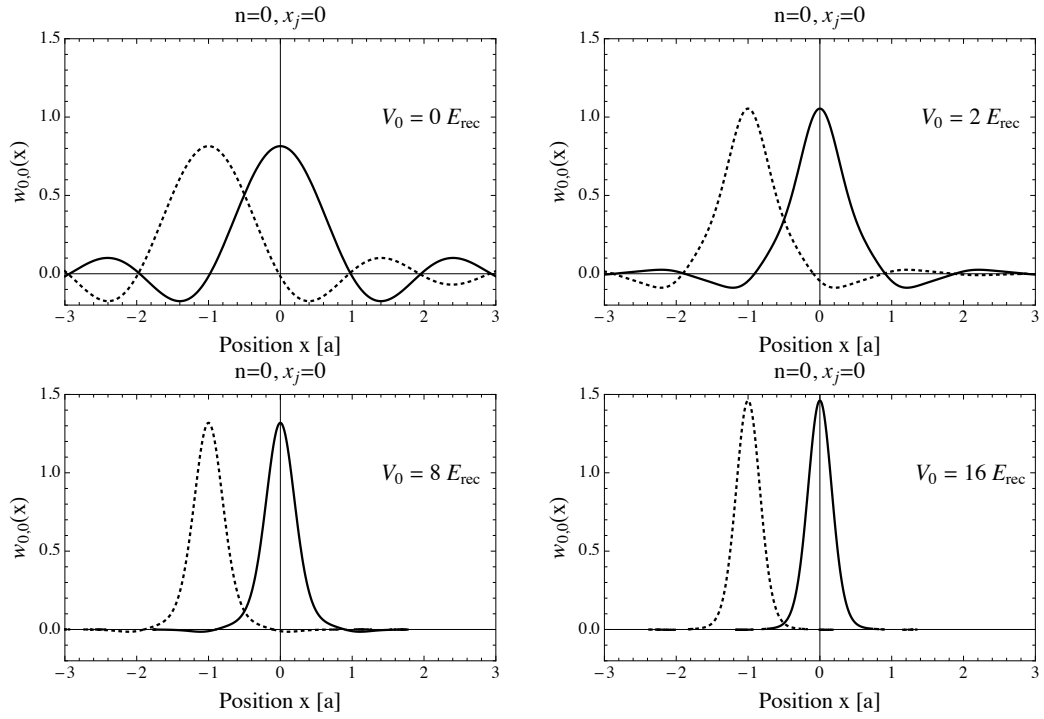

Figure 13: Amplitude of the Wannier functions in the fundamental band $W_{n=0,j}(x)$ for $j = 0$ (full lines) and $j = -1$ (dashed lines) for $V_0 = 0, 2, 8, 16\, E_{\rm rec}$.

3.2 Hamiltonian in terms of Wannier functions

We will now give another expression of the Hamiltonian using the Wannier functions, which is particularly relevant in the tight-binding regime. The idea is to give the Hamiltonian under a second quantized form for bosons using creation and anihilation operators in a given Wannier state.

We start with the Bloch states $|\psi_{n,q}\rangle$, which are the eigenstates of $\hat{H}$. We introduce the operators $\hat{a}_{n,q}$ and $\hat{a}^\dagger_{n,q}$ which anihilate and create an atom in the Bloch state $|\psi_{n,q}\rangle$, respectively. We describe bosons here such that the operators obey the bosonic commutation relations

$$\left[\hat{a}_{n,q}, \hat{a}^\dagger_{n',q'}\right] = \delta_{n,n'}\tilde{\delta}_{q,q'}.$$

The Hamiltonian can then be written as

$$\hat{H} = \sum_n \sum_{q\in \mathrm{FBZ}} E_n(q)|\psi_{n,q}\rangle\langle\psi_{n,q}| = \sum_n \sum_{q\in \mathrm{FBZ}} E_n(q)\hat{a}^\dagger_{n,q}\hat{a}_{n,q}. \tag{24}$$

If we now introduce the operators $\hat{b}_{n,j}$ and $\hat{b}^\dagger_{n,j}$ which anihilate and create an atom in the Wannier state $|W_{n,j}\rangle$, the $\hat{a}_{n,q}$ and $\hat{b}_{n,j}$ are linked by a relation similar to Eq. (22):

$$\hat{a}_{n,q} = \frac{1}{\sqrt{N_s}} \sum_j \hat{b}_{n,j}\, e^{ijqa}. \tag{25}$$

Let us substitute Eq. (25) into the Hamiltonian Eq. (24):

$$\hat{H} = \frac{1}{N_s} \sum_n \sum_{j,j'} \hat{b}^\dagger_{n,j}\hat{b}_{n',j'} \sum_{q\in \mathrm{FBZ}} E_n(q)\, e^{i(j'-j)qa}$$

$$\boxed{\hat{H} = \sum_n \sum_{j,j'} J_n(j'-j)\, \hat{b}^\dagger_{n,j} \hat{b}_{n',j'}} \tag{26}$$

where

$$\boxed{J_n(j) = \frac{1}{N_s} \sum_{q \in \mathrm{FBZ}} E_n(q)\, e^{ijqa} \underset{L\to\infty}{=} \frac{a}{2\pi} \int_{-\frac{\pi}{a}}^{\frac{\pi}{a}} E_n(q)\, e^{ijqa}\, \mathrm{d}q.} \tag{27}$$

The second expression is obtained when we let L or $N_s \to \infty$. $J(j)$ is real due to the symmetry of $E_n(q)$. It describes the hopping within band n between sites separated by a distance ja:

$$J_n(j) = \langle W_{n,j} | \hat{H} | W_{n,0} \rangle.$$

Using Fourier transform we can write in the limit $N_s \to \infty$

$$E_n(q) = \sum_j J_n(j)\, e^{-ijqa} = J_n(0) + \sum_{j=1}^{\infty} J_n(j) \cos(jqa). \tag{28}$$

$J_n(0)$ is the average value of E_n on the FBZ. $J_n(j)$ decreases rapidly with j.

In the fundamental band, as soons as $V_0 > E_{\mathrm{rec}}$, we can write

$$E_0(q) \simeq J_0(0) - 2J\cos(qa)$$

where we have defined

$$J = -J_0(1) = -\frac{1}{N_s} \sum_{q \in \mathrm{FBZ}} E_0(q)\, e^{iqa} \underset{L\to\infty}{=} -\frac{a}{2\pi} \int_{-\frac{\pi}{a}}^{\frac{\pi}{a}} E_0(q)\, e^{iqa}\, \mathrm{d}q. \tag{29}$$

The minus sign is introduced such that $J > 0$. The energy width of the fundamental band is approximately $4J$.

3.3 Bose-Hubbard Hamiltonian

The Hamiltonian (26) describes the dynamics of non interacting bosons in the lattice. This form is well appropriate to now add the interations between the bosons, within some approximations.

We will consider the case of a lattice deep enough ($V_0 > E_{\mathrm{rec}}$) and energies small enough in order to restrict the description to the lowest band ($n = 0$) and neglect hopping to distant sites, namely $J_0(j)$ for $j \geq 2$. As $J_0(0)$ is an irrelevant offset of the energies we will also drop it. We will also omit the $n = 0$ index in the $\hat{b}$ operators. The Hamiltonian for non interacting particles thus writes

$$\hat{H} = -J \sum_j (\hat{b}^\dagger_j \hat{b}_{j+1} + \hat{b}^\dagger_j \hat{b}_{j-1}) = -J \sum_j \hat{b}^\dagger_{j+1} \hat{b}_j + \mathrm{h.c.}$$

The interaction term of the Hamiltonian, if we assume contact interactions $V_{\mathrm{int}}(\mathbf{r}, \mathbf{r}') = g\delta(\mathbf{r} - \mathbf{r}')$, writes in second quantization

$$\hat{H}_{\mathrm{int}} = \frac{g}{2} \int \hat{\psi}^\dagger(x) \hat{\psi}^\dagger(x) \hat{\psi}(x) \hat{\psi}(x)\, \mathrm{d}x.$$

We now write the field operator $\hat{\psi}(x)$ in terms of Wannier operators

$$\hat{\psi}(x) = \sum_{n,j} W_{n,j}(x)\hat{b}_{n,j}.$$

This will give for $\hat{H}_{\text{int}}$ a sum on $n_1n_2n_3n_4$ and $j_1j_2j_3j_4$ of overlap integrals of Wannier functions. For interaction energies small enough, the system always stays in the lowest band such that $n_i = 0$. In addition, for V_0 larger than a few E_{rec}, the extension of $W_{0,j}$ to the next well $j \pm 1$ is very small (see Fig. 13) such that the overlap integral will be vanishingly small unless $j_1 = j_2 = j_3 = j_4 = j$. We are thus left with

$$\hat{H}_{\text{int}} = \frac{g}{2}\sum_j \hat{b}_j^\dagger\hat{b}_j^\dagger\hat{b}_j\hat{b}_j \int W_{0,j}^4 \,\mathrm{d}x = \frac{g}{2}\sum_j \hat{b}_j^\dagger\hat{b}_j^\dagger\hat{b}_j\hat{b}_j \int W_{0,0}^4 \,\mathrm{d}x.$$

We introduce the operator $\hat{n}_j = \hat{b}_j^\dagger\hat{b}_j$ which counts the number of particles in state $|W_{0,j}\rangle$. Using the bosonic commutation relations, we can derive the interaction term

$$\boxed{\hat{H}_{\text{int}} = \frac{U}{2}\sum_j \hat{n}_j(\hat{n}_j - 1)} \tag{30}$$

where

$$\boxed{U = g\int W_{0,0}^4 \,\mathrm{d}x.} \tag{31}$$

The total Hamiltonian then reads

$$\boxed{\hat{H}_{\text{BH}} = -J\sum_j \hat{b}_{j+1}^\dagger\hat{b}_j + \text{h.c.} + \frac{U}{2}\sum_j \hat{n}_j(\hat{n}_j - 1).} \tag{32}$$

It is called the **Bose-Hubbard Hamiltonian**.

3.4 Mott transition

The ground state of the Bose-Hubbard Hamiltonian depends on the relative weight of the kinetic (J) and interaction (U) term. We can give an estimation of U by approximating $W_{0,0}$ as the ground state of an harmonic oscilltor at the bottom of a lattice well, with the frequency ω_0 given by Eq. (13):

$$U \simeq \frac{g}{\sqrt{2\pi}a_0} \qquad \text{where} \quad a_0 = \sqrt{\frac{\hbar}{M\omega_0}} = \frac{1}{k}\left(\frac{E_{\text{rec}}}{V_0}\right)^{1/4}$$

In the 3D case, we find

$$U \simeq \frac{g}{(2\pi)^{3/2}a_0^3}.$$

Using the expression of g in the frame of s-wave collisions with scattering length a_s:

$$g = \frac{4\pi\hbar^2 a_s}{M}, \tag{33}$$

we get for the 3D case

$$\frac{U}{E_{\text{rec}}} \simeq \sqrt{\frac{8}{\pi}}ka_s\left(\frac{V_0}{E_{\text{rec}}}\right)^{3/4}. \tag{34}$$

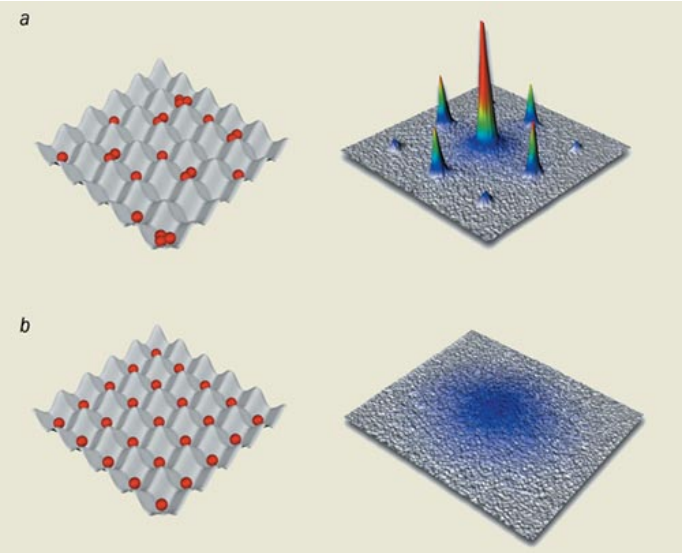

Figure 14: Observation of the Mott transition with a quantum gas. Diffraction peaks are present at low V_0, when the state is coherent and the number of particles per site fluctuates. They disappear at large V_0 when coherence is lost and the number of particles per site is equal to the filling factor ν. Figure from [6].

An estimate for J in the limit $V_0 \gg E_{\rm rec}$ is given by

$$\frac{J}{E_{\rm rec}} \simeq \sqrt{\frac{4}{\pi}} \left(\frac{V_0}{E_{\rm rec}}\right)^{3/4} e^{-2\sqrt{V_0/E_{\rm rec}}}. \tag{35}$$

It follows that the ratio of J and U depends exponentially on $\sqrt{V_0}$:

$$\frac{J}{U} \simeq \frac{\sqrt{2}}{k a_s} e^{-2\sqrt{V_0/E_{\rm rec}}}. \tag{36}$$

It is therefore quite easy to modify strongly this ratio, from a regime $J \gg U$ where interactions play little role to an interaction-dominated regime for $U \gg J$. For example, with rubidium atoms in a lattice with $k \sim k_0$ where $\lambda_0 = 2\pi/k_0$ is the resonance wavelength at 780 nm, $J/U \simeq 40 \exp[-2\sqrt{V_0/E_{\rm rec}}]$ and the transition from a regime to the other occurs around $V_0 \simeq 16\, E_{\rm rec}$.

The Mott transition is a quantum phase transition, occuring at zero temperature, from a conducting state (for electrons in a solid) to an insulating state as the interaction strength increases. It occurs for a critical value of J/U. By analogy, it has been proposed by Jaksch et al. [18] to observe it with cold gases in optical lattices. The transition here occurs between a superfluid state for high J/U and a localized (or insulating) state for low J/U.

Consider the situation where we have N particles spread in the N_s sites of the lattice, which corresponds to a filling factor $\nu = N/N_s$. At low V_0, for $J/U > (J/U)_c$, kinetic energy dominates, the many-body wave function of the particles is close to the product state of Bloch states corresponding to noninteracting particles, i.e. we have all N particles in a Bloch state:

$$|\psi\rangle_{\rm SF} \simeq \frac{1}{\sqrt{N!}} \left(\hat{a}_q^\dagger\right)^N |0\rangle$$

with $q = 0$ for the ground state. It is delocalized and coherent over the whole lattice:

$$\langle \hat{b}_j^\dagger \hat{b}_{j'} \rangle = \nu e^{i(j-j')qa} \Rightarrow \left| \langle \hat{b}_j^\dagger \hat{b}_{j'} \rangle \right| = \nu.$$

Diffraction peaks are visible in a time-of-flight experiment, see Fig. 14. Simple algebra shows that the average number of particles in each well is equal to the filling, $\langle \hat{n}_j \rangle = \langle \hat{b}_j^\dagger \hat{b}_j \rangle = \nu$ but this number fluctuates with Poissonian statistics:

$$\Delta n_j = \sqrt{\langle \hat{n}_j^2 \rangle - \langle \hat{n}_j \rangle^2} = \sqrt{\nu \left(1 - \frac{1}{N_s}\right)} \simeq \sqrt{\nu} = \sqrt{\langle \hat{n}_j \rangle}.$$

On the other hand, for larger V_0 such that $J/U < (J/U)_c$, the interaction energy dominates and the ground state is determined by its minimization, which corresponds to having the same number of particle per site. In particular if the filling is an integer number ν, the ground state corresponds to a fixed number ν of particles per site and writes

$$|\psi\rangle_{\text{Mott}} = |\nu, \nu, \ldots, \nu\rangle = \prod_j \frac{1}{\sqrt{\nu!}} \left(\hat{b}_j^\dagger\right)^\nu |0\rangle.$$

This can be understood by comparing the interation energy in two situations: (i) ν particles in two neighbouring sites or (ii) $\nu - 1$ in one and $\nu + 1$ in the other:

$$E_{(i)} = 2 \times \frac{U}{2} \nu(\nu - 1) = U(\nu^2 - \nu) \qquad E_{(ii)} = \frac{U}{2}(\nu - 1)(\nu - 2) + \frac{U}{2}\nu(\nu + 1) = U(\nu^2 - \nu + 1)$$

We find that $E_{(ii)} > E_{(i)}$ and the difference is exactly U. The particles are frozen in the wells, and this state is called a **Mott insulator**. The average $\langle \hat{n}_j \rangle$ is still ν, but now the fluctuations vanish:

$$\langle \hat{n}_j^2 \rangle = \langle \hat{b}_j^\dagger \hat{b}_j \hat{b}_j^\dagger \hat{b}_j \rangle = \langle \hat{b}_j^\dagger \hat{b}_j^\dagger \hat{b}_j \hat{b}_j \rangle + \langle \hat{b}_j^\dagger \hat{b}_j \rangle = \nu(\nu - 1) + \nu = \nu^2 = \langle \hat{n}_j \rangle^2 \Rightarrow \Delta n_j = 0.$$

On the contrary, the relative phase between wells, which is related to its conjugate variable, is undetermined:

$$\langle \hat{b}_j^\dagger \hat{b}_{j'} \rangle = \nu \delta_{j,j'}.$$

Superfluidity is destroyed and the system is in a highly correlated many-body state, not a Bloch state common to all atoms. Diffraction peaks disappear in a time-of-flight experiment, see Fig. 14.

Strictly speaking, the Mott transition would only occur at integer filling. If the atoms are confined in a large scale trap on top of the lattice, however, the local value of the chemical potential depends on the position – larger at the center where the atoms gather and smaller towards the edge. As a result, the gas organises into concentric zones where the filling is fixed and the state is an insulator, with small transition regions which absorb all the fluctuations. This structure with shells resembles a wedding cake, see Fig. 15.

3.5 Noise correlations in the Mott phase

We could wonder if the smearing of the diffraction peak is a sufficient proof for a Mott state, and not instead due to some experimental imperfection. A first argument for the quality of the state preparation is that the diffraction peaks are recovered if the lattice

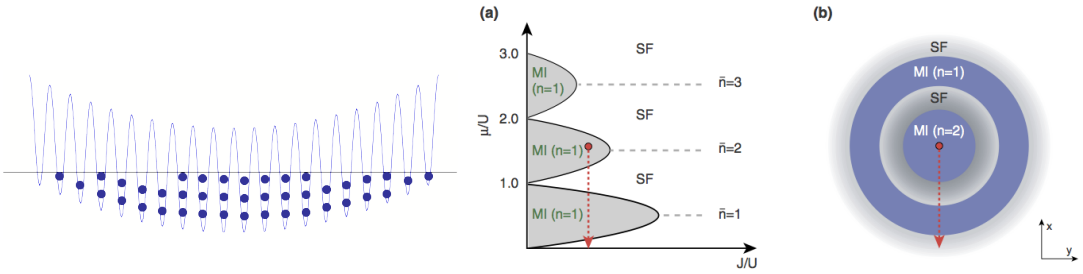

Figure 15: Mott shells for an inhomogeneous quantum gas in the presence of an external harmonic trap. Left: for a chemical potential μ_0 at the center, the local chemical potential $\mu = \mu_0 - V_{\rm ext}(\mathbf{r})$ varies across the trap, and so does the average filling factor. Right: At fixed J/U, starting from the edges, the system spans all values of μ/U betwenn 0 and μ_0/U and goes across several Mott zone with $\nu = 1, 2, 3\ldots$ Figure from [7].

amplitude is ramped back to below the transition threshold. Another evidence takes advantage of the noise correlations in the Mott phase.

Let us write the evolution of the wave function in a time-of-flight experiment in the Wannier basis. We get after a time $t_{\rm TOF}$:

$$\begin{aligned}\hat{\psi}(\mathbf{r}, t_{\rm TOF}) &= \sum_j W(\mathbf{r} - \mathbf{r}_j, t_{\rm TOF})\hat{b}_j \\ &= \left(\frac{M}{\hbar t_{\rm TOF}}\right)^{3/2} \tilde{W}\left(\mathbf{k} = \frac{M\mathbf{r}}{\hbar t_{\rm TOF}}\right) \sum_j e^{i\mathbf{k}\cdot\mathbf{r}_j}\hat{b}_j.\end{aligned}$$

The momentum distribution $n(\mathbf{k})$ of the gas is linked to the position distribution after the time-of-flight using the relation $\mathbf{r} = t_{\rm TOF} \times \hbar\mathbf{k}/M$. It is also the Fourier transform of the first order correlation. If we ignore the broad envelope $|\tilde{W}(\mathbf{k})|^2$ linked to the Fourier transform of the initial size inside each well, we get

$$n(\mathbf{k}) = \langle\hat{\psi}^\dagger(\mathbf{k})\hat{\psi}(\mathbf{k})\rangle \propto \sum_{i,j} e^{i\mathbf{k}\cdot(\mathbf{r}_j - \mathbf{r}_i)}\langle\hat{b}_i^\dagger\hat{b}_j\rangle = S(\mathbf{k}).$$

$S(\mathbf{k})$ is the *structure factor*. In the Mott phase, $S(\mathbf{k}) = \nu N_s = N$: the momentum distribution is flat in the Mott phase. Density correlations computed on a time-of-flight picture give access to *second order* momentum correlations in the Mott state, i.e.:

$$\langle n(\mathbf{k})n(\mathbf{k}')\rangle = \langle\hat{\psi}^\dagger(\mathbf{k})\hat{\psi}(\mathbf{k})\hat{\psi}^\dagger(\mathbf{k}')\hat{\psi}(\mathbf{k}')\rangle \propto \sum_{i,j,\ell,m} e^{i\mathbf{k}\cdot(\mathbf{r}_j - \mathbf{r}_i)}e^{i\mathbf{k}'\cdot(\mathbf{r}_m - \mathbf{r}_\ell)}\langle\hat{b}_i^\dagger\hat{b}_j\hat{b}_\ell^\dagger\hat{b}_m\rangle.$$

We can compute $\langle\hat{b}_i^\dagger\hat{b}_j\hat{b}_\ell^\dagger\hat{b}_m\rangle$ in the Mott phase with filling ν. Using the commutation relations, this writes

$$\langle\hat{b}_i^\dagger\hat{b}_j\hat{b}_\ell^\dagger\hat{b}_m\rangle = \langle\hat{b}_i^\dagger\hat{b}_\ell^\dagger\hat{b}_j\hat{b}_m\rangle + \delta_{j,\ell}\langle\hat{b}_i^\dagger\hat{b}_m\rangle = \mathcal{C} + \mathcal{C}_{\rm auto}.$$

The contribution of the second term $\mathcal{C}_{\rm auto}$ reads

$$\sum_{i,j,\ell,m} e^{i\mathbf{k}\cdot(\mathbf{r}_j - \mathbf{r}_i)}e^{i\mathbf{k}'\cdot(\mathbf{r}_m - \mathbf{r}_\ell)}\delta_{j,\ell}\langle\hat{b}_i^\dagger\hat{b}_m\rangle = \sum_{i,m} e^{-i\mathbf{k}\cdot\mathbf{r}_i}e^{i\mathbf{k}'\cdot\mathbf{r}_m}\langle\hat{b}_i^\dagger\hat{b}_m\rangle \sum_j e^{i(\mathbf{k}-\mathbf{k}')\cdot\mathbf{r}_j} = N_s\delta_{\mathbf{k},\mathbf{k}'}S(\mathbf{k}).$$

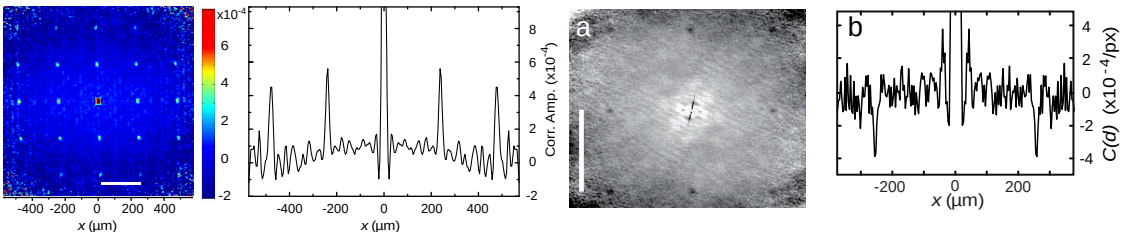

Figure 16: Correlations in the density distribution after a time-of-flight, which measure the momentum second order correlations. Left, from [19]: bosons in the Mott phase, with positive correlations at momenta corresponding to multiples of $2\hbar k$. Right, from [20]: fermions in the Mott phase, the correlation is negative at $\pm 2\hbar k$ because of the fermionic statistic.

It is the autocorrelation, which is always present. We now concentrate on the first term, which is zero unless $j = i$ and $m = \ell$, or $j = \ell$ and $m = i$, or all the indices are equal. In the Mott phase with ν particles per site, it reads

$$\mathcal{C} = \langle \hat{b}_i^\dagger \hat{b}_\ell^\dagger \hat{b}_j \hat{b}_m \rangle = \nu^2 \left(\delta_{i,j}\delta_{\ell,m} - \delta_{i,j,\ell,m}\right) + \nu^2 \left(\delta_{i,m}\delta_{j,\ell} - \delta_{i,j,\ell,m}\right) + \nu(\nu-1)\delta_{i,j,\ell,m}.$$

Finally

$$\mathcal{C} = \nu^2 \delta_{i,j}\delta_{\ell,m} + \nu^2 \delta_{i,m}\delta_{j,\ell} - \nu(\nu+1)\delta_{i,j,\ell,m}.$$

We get

$$\langle n(\mathbf{k}) n(\mathbf{k}') \rangle \propto \nu^2 N_s^2 + \nu^2 \sum_{i,j} e^{i(\mathbf{k}-\mathbf{k}')\cdot(\mathbf{r}_j - \mathbf{r}_i)} - \nu(\nu+1) N_s.$$

The normalized correlation function is obatined after dividing by $\nu^2 N_s^2$:

$$g^{(2)}(\mathbf{k}, \mathbf{k}') = 1 + \frac{1}{N_s^2} \sum_{i,j} e^{i(\mathbf{k}-\mathbf{k}')\cdot(\mathbf{r}_j - \mathbf{r}_i)} - \frac{\nu+1}{\nu} \frac{1}{N_s}.$$

When N_s is large, the last term is negligible. The second term vanishes, unless $\mathbf{k} - \mathbf{k}'$ belongs to the reciprocal lattice, and in this case this term is 1, on the same order than the first term. The regular underlying structure of the Mott phase is revealed in the density correlations after a time-of-flight, as is clear from Fig. 16.

When fermions are used instead of bosons, a Mott phase also exists. The first swap between $\hat{b}_j$ and $\hat{b}_\ell^\dagger$ introduces a minus sign. As a result, we know observe *anti-correlations* when the momenta differ by a vector of the reciprocal lattice, see Fig. 16.

References

[1] Phillip L. Gould, George A. Ruff and David E. Pritchard, Diffraction of atoms by light: The near-resonant Kapitza-Dirac effect. *Phys. Rev. Lett.* **56**, 827–830 (Feb 1986).

[2] G. Grynberg and C. Robilliard, Cold atoms in dissipative optical lattices. *Physics Reports* **355**, 335 – 451 (2001).

[3] M. Greiner, O. Mandel, T. W. Hänsch and I. Bloch, Quantum Phase Transition from a Superfluid to a Mott Insulator in a Gas of Ultracold Atoms. *Nature* **415**, 39 (2002).

[4] Immanuel Bloch, Jean Dalibard and Sylvain Nascimbène, Quantum simulations with ultracold quantum gases. *Nature Physics* **8**, 267– (April 2012).

[5] Hidetoshi Katori, Masao Takamoto, V. G. Pal'chikov and V. D. Ovsiannikov, Ultrastable Optical Clock with Neutral Atoms in an Engineered Light Shift Trap. *Phys. Rev. Lett.* **91** (17), 173 005 (Oct 2003).

[6] I. Bloch, Ultracold quantum gases in optical lattices. *Nature Physics* **1**, 23 (2005).

[7] Markus Greiner, *Ultracold quantum gases in three-dimensional optical lattice potentials* PhD thesis, Ludwig-Maximilians-Universität München (2003).

[8] Jean Dalibard, Des cages de lumière pour les atomes : la physique des pièges et des réseaux optiques (2013). Cours au Collège de France.

[9] R. Grimm, M. Weidemüller and Yu. B. Ovchinnikov, Optical dipole traps for neutral atoms. *Adv. At. Mol. Opt. Phys.* **42**, 95–170 (2000).

[10] P. Lemonde, Optical lattice clocks. *The European Physical Journal Special Topics* **172** (1), 81–96 (Jun 2009).

[11] W. Ketterle, D. S. Durfee and D. M. Stamper-Kurn, Making, probing and understanding Bose-Einstein condensates. In *Proceedings of the International School of Physics "Enrico Fermi", Course CXL*, edited by M. Inguscio, S. Stringari and C. E. Wieman, pages 67–176, IOS Press Ohmsha (1999). https://arxiv.org/abs/cond-mat/9904034.

[12] Maxime Ben Dahan, Ekkehard Peik, Jakob Reichel, Yvan Castin and Christophe Salomon, Bloch Oscillations of Atoms in an Optical Potential. *Phys. Rev. Lett.* **76**, 4508–4511 (Jun 1996).

[13] Rémy Battesti, Pierre Cladé, Saïda Guellati-Khélifa, Catherine Schwob, Benoît Grémaud, François Nez, Lucile Julien and François Biraben, Bloch Oscillations of Ultracold Atoms: A Tool for a Metrological Determination of h/m_{Rb}. *Phys. Rev. Lett.* **92**, 253 001 (Jun 2004).

[14] M. Gustavsson, E. Haller, M. J. Mark, J. G. Danzl, G. Rojas-Kopeinig and H.-C. Nägerl, Control of Interaction-Induced Dephasing of Bloch Oscillations. *Phys. Rev. Lett.* **100**, 080 404 (Feb 2008).

[15] Ekkehard Peik, Maxime Ben Dahan, Isabelle Bouchoule, Yvan Castin and Christophe Salomon, Bloch oscillations of atoms, adiabatic rapid passage, and monokinetic atomic beams. *Phys. Rev. A* **55**, 2989–3001 (Apr 1997).

[16] Pierre Cladé, Saïda Guellati-Khélifa, François Nez and François Biraben, Large Momentum Beam Splitter Using Bloch Oscillations. *Phys. Rev. Lett.* **102** (24), 240 402 (Jun 2009).

[17] Holger Müller, Sheng-wey Chiow, Sven Herrmann and Steven Chu, Atom Interferometers with Scalable Enclosed Area. *Phys. Rev. Lett.* **102**, 240 403 (Jun 2009).

[18] D. Jaksch, C. Bruder, J. I. Cirac, C. W. Gardiner and P. Zoller, Cold Bosonic Atoms in Optical Lattices. *Phys. Rev. Lett.* **81**, 3108–3111 (Oct 1998).

[19] Simon Fölling, Fabrice Gerbier, Artur Widera, Olaf Mandel, Tatjana Gericke and Immanuel Bloch, Spatial quantum noise interferometry in expanding ultracold atom clouds. *Nature* **434** (7032), 481–484 (2005).

[20] T. Rom, Th. Best, D. van Oosten, U. Schneider, S. Fölling, B. Paredes and I. Bloch, Free fermion antibunching in a degenerate atomic Fermi gas released from an optical lattice. *Nature* **444** (7120), 733–736 (2006).